



Phase inconsistency as a major source of error in NGFS forecast

Priyanshi Singhai¹ · Shibin Balakrishnan² · E. N. Rajagopal³ · Arindam Chakraborty¹

Received: 31 May 2019 / Accepted: 24 January 2020 / Published online: 4 February 2020

© Springer-Verlag GmbH Germany, part of Springer Nature 2020

Abstract

South Asian monsoon exhibits multiscale spatiotemporal variability. Analyzing the nature and behavior of numerical weather forecast error associated with these space-time heterogeneities will eventually help in improving the models. We investigate the spatiotemporal error characteristics of the National Centre for Medium-Range Weather Forecasting (NCFMRWF) Global Forecast System (NGFS) model over South Asian land and ocean separately. Although error grows with lead-time, it saturates within 3–5 days of forecast initiation. The saturated error is only about 15–25% higher than that of day-1, indicating that most of the error accumulates within first 24-h of forecast. Increase in error over oceanic regions is due to an increase in the area with high error at all precipitation ranges with large day-to-day variability. However, over land error growth is primarily confined at locations of high mean precipitation. Decomposition of error arising due to intensity and phase variations reveals that about 90% of it arises from the model's inability to capture phase of precipitation at various timescales. We show that NGFS cannot capture synoptic scale variations (< 10 day) after day-2. Both the high-frequency (10–20 day) and low-frequency (30–60 day) intraseasonal variations are reasonably predicted up to day-3. At diurnal timescale, NGFS forecasts show a peak in precipitation about 3–6 h prior to that observed, both over land and ocean. Surprisingly, this error does not change with lead-time. Lastly, we show that major error characteristics do not depend on the seasonal mean monsoon rainfall.

Keywords Short-to-medium range forecast · Indian monsoon · Diurnal cycle · Phase error

1 Introduction

Boreal summer precipitation [June–September; (JJAS)] serves as the life-giving rainfall for the agrarian economies of South Asian countries. It exhibits a broad band of spatiotemporal variability. Its accurate prediction at high spatial and temporal resolution using dynamical models has remained a challenging task (Gadgil et al. 2005; Gadgil and Srinivasan 2012), in spite of several advances in the numerical weather prediction (NWP) models, observations as well

as data assimilation schemes (Simmons and Hollingsworth 2002; Harper et al. 2007; Kalnay et al. 1998). Thus, it is necessary to understand the usefulness and reasons behind the shortcomings of the NWP model over this region.

Errors in short-to-medium range prediction of the South Asian summer monsoon could be a result of inconsistent initial conditions, coarse resolution of the models, inadequate representation of convection, and missing air-sea coupling. In recent studies, it has been suggested that increasing resolution does not necessarily guarantee an improvement in the forecast skill (Tibaldi et al. 1990; Mass et al. 2002; Sahai et al. 2014). One important issue associated with high resolution is that small phase error in the forecast is penalized twice, once for missing the observation and once again for giving a false alarm (Anthes 1983). This is known as “Double Penalty”. This can lead to high spatiotemporal error in the high resolution forecast. Misrepresentation of energy fluxes between the atmosphere and land/ocean (Fu et al. 2002, 2008; Li et al. 2018), and land surface processes (Beljaars et al. 1996) can also lead to different error characteristics over land and ocean. Therefore understanding the error

Electronic supplementary material The online version of this article (<https://doi.org/10.1007/s00382-020-05148-y>) contains supplementary material, which is available to authorized users.

Priyanshi Singhai
priyanshis@iisc.ac.in

¹ Centre for Atmospheric and Oceanic Sciences, and Divecha Centre for Climate Change, Indian Institute of Science, Bengaluru 560012, Karnataka, India

² India Meteorological Department, New Delhi 110037, India

³ National Centre for Medium Range Weather Forecasting, Noida 201309, Uttar Pradesh, India

behavior can help us to improve the physical process causing the error, thus eventually improves the weather forecast.

Several previous studies have delineated the variability of model forecast error in space and time. Lee Drbohlav and Krishnamurthy (2010) and Pavan and Doblas-Reyes (2000) showed that the origin, nature, and intensity of the forecast error vary spatially and temporally. The skill of the NWP model is also dependent on the physics of the model (Krishnamurti et al. 1999; Chakraborty et al. 2007; Taraphdar et al. 2016). Model's skill has been traditionally evaluated using root-mean-square error, correlation coefficient (Anthes 1983). Recent studies have employed methods like filtering and displacement (Gilleland et al. 2009). Ebert and McBride (2000) and Ebert and Gallus Jr (2009) decomposed the total spatial error into displacement, volume, and pattern of the precipitation forecast using a feature-based approach (a type of displacement method) and suggested that location error is the dominant source of error. This method, however, does not account for the error arising due to temporal variation. On the other hand, Colle et al. (2001) showed that the forecast error in the NWP model could be primarily attributed to the timing (phase) of the forecasted parameter. Their study also suggests that the scale interaction between the error having shorter timescales results in a large error of the seasonally forecasted variable, leading to poor forecasting skills of the model. Slingo et al. (2003) suggested that the systematic error in the model is associated with the improper representation of the diurnal cycle in the model. Chakraborty (2010) also attributed that poor forecast over the Indian region is due to incorrect phase-locking of the diurnal cycle in the ECMWF model. Thus, a quantitative delineation between intensity and phase of error is missing.

Under the National monsoon mission, NGFS has been identified as a potential forecast system for the prediction of the Indian summer monsoon. NGFS is an atmospheric model with a coupled land-atmosphere dynamics and prescribed sea surface temperature for all days of the forecast. Hence, it is necessary to analyze the error characteristic of the NGFS model over land and ocean separately. The objective of this study is to address the following:

- Understanding the spatial and temporal variability of error of the NGFS model over land and ocean separately.
- Is there any difference in error behavior over land and ocean?
- What are the dominant causes of error in this model, mean intensity or phase?
- How well does the model depict the scale interactions at various timescales?

This paper is organized as follows. Section 2 describes the model and observational dataset. Section 3 outlines the methodology used in this paper. In Sect. 4 we have discussed

our results in detail, followed by conclusions of this work in Sect. 5.

2 Model description and data sets

We utilize National Centre for Medium-Range Weather Forecasting (NCMRWF) Global Forecasting System (NGFS) version 9.0.1, which is developed at the Environmental Modelling Center (EMC) of National Centers for Environmental Predictions (NCEP) and further modified at the NCMRWF. NGFS is a spectral model. We use a version of the model with triangular truncation at 574 waves (T574) in the zonal direction. The model uses Gaussian quadrature in latitudes for accurate computation. These translate to approximately $0.20^\circ \times 0.21^\circ$ resolution in grid space. In the vertical direction, there are 64 unequally spaced hybrid sigma levels (L64). The model is integrated for 7 days starting at 00 GMT every day from 1 June through 30 September 2012 and 2013.

The observation precipitation data used is TRMM-3B42 (Huffman et al. 2007), which is a satellite-based precipitation product and is referred as TRMM in this study. It is available at a temporal resolution of 3-h and a spatial resolution of $0.25^\circ \times 0.25^\circ$. To compare NGFS with TRMM precipitation, we regrid the model output to TRMM resolution using bilinear interpolation.

3 Methodology

The NGFS model output is available at a temporal resolution of 3-h from 0 to 168 h. We have averaged all 3-hourly output from 0000 to 2100 GMT to create a daily mean dataset. Since forecasts at all lead-time (day 1 through day 7) are available from 7 June–30 September (116 days), we carried out our analysis for this period. We term model forecasts of the first 24 h as day-1, next 24 h as day 2, and so on.

For seasonal and intraseasonal analysis, the string of day-1 forecasts, starting at every initial condition from 7 June through 30 September constitute the daily time series of the day-1 forecast. Longer lead times follow similarly. We average 116-forecasts at every 3-h (0–3, 3–6, ..., 21–24) and every lead-day (days 1 through 7) for skill evaluation at diurnal time scales. We have referred precipitation between 00–03 GMT as 00 GMT, 03–06 as 03 GMT, ..., 21–24 as 21 GMT throughout the paper. We employ harmonic analysis to extract the leading diurnal mode at each forecast lead day. To extract intraseasonal signal at a certain frequency band, we at first decomposed time series using harmonic analysis and retained frequencies corresponding to the time period concerned. These are further discussed in the respective section (4.2.1 and 4.2.2). The first part of analysis is

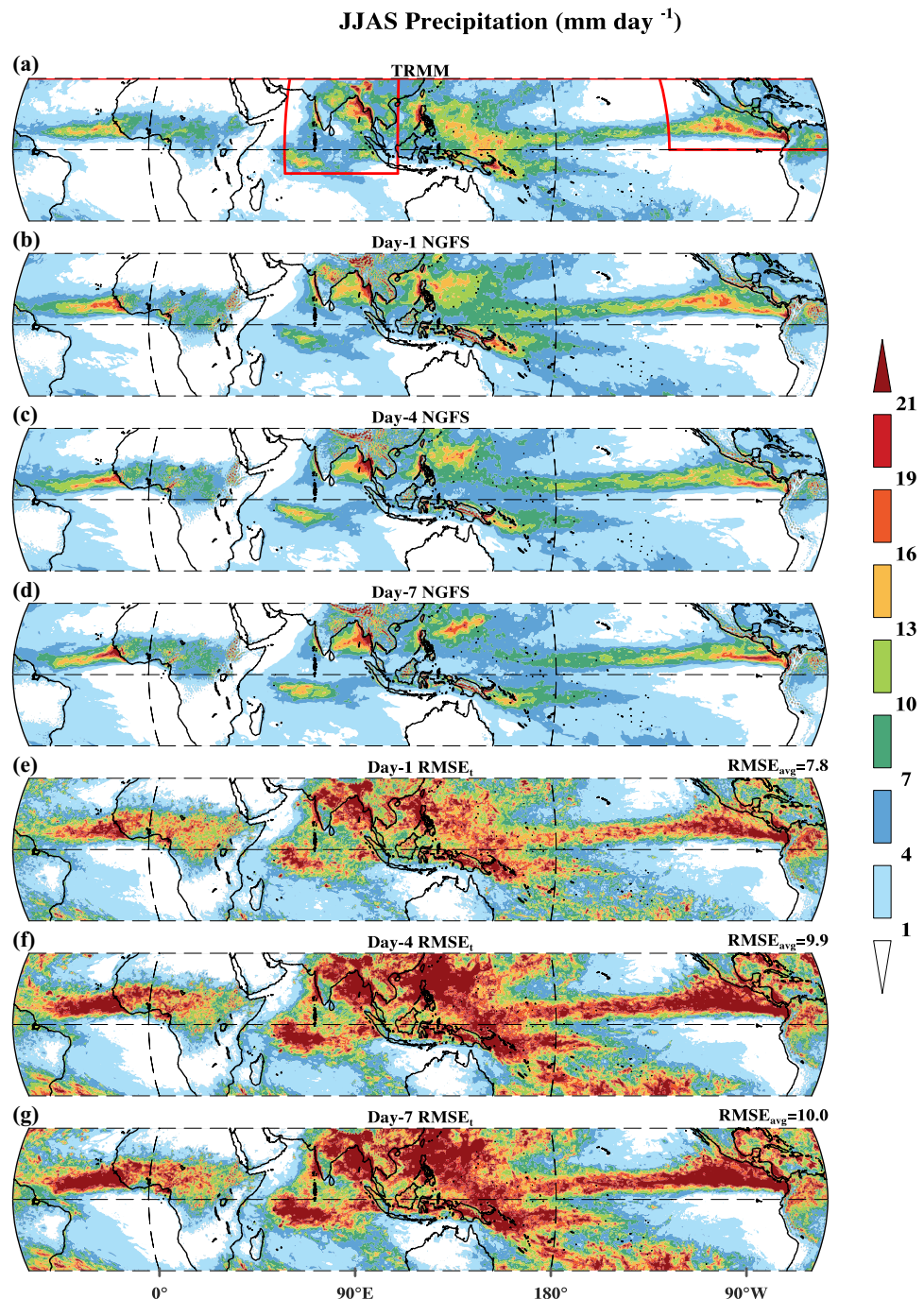
based on the forecast for 2012 (Sects. 4.1–4.3). Major error characteristics of the same year are compared with 2013 in Sect. 4.4.

4 Results

Figure 1a–d show boreal summer (June–September) mean precipitation over the tropics (30° S– 30° N, 0° E– 360° E) from TRMM-3B42 estimates and NGFS forecasts for days

1, 4, and 7, respectively. General features of the tropical precipitation such as the tropical convergence zone, orographic rainfall (the Western Ghats, foothills of the Himalayas, and Myanmar), and the South Pacific convergence zone are captured reasonably well by the model both in terms of intensity and spatial pattern. The NGFS model tends to underestimate the precipitation over the north Bay of Bengal, western and eastern equatorial Pacific ocean, while it overestimates over south-west Bay

Fig. 1 Precipitation (mm day^{-1}) from **a** TRMM estimate, **b–d** NGFS forecasts for days 1, 4, and 7 averaged over June–September 2012, **e–g** RMS Error (mm day^{-1}) in time for days 1, 4, and 7 forecast over the tropics for the same time period. Also, area-averaged RMS error over the same domain is shown at the top of **e–g**



of Bengal, northeast India, and over Myanmar. These pros and cons of NGFS are consistent at all lead times.

To understand how well the model captures day-to-day variability, we have shown in Fig. 1e–g the spatial distribution of root mean square error of temporal variations of precipitation ($RMSE_t$) defined as:

$$RMSE_t = \sqrt{\frac{1}{N} \sum_{i=1}^N (M_i - O_i)^2} \quad (1)$$

where N is the total number of time points (116 daily averages from 7 June to 30 September); M_i and O_i are model and observed precipitation, respectively, on the i th day. $RMSE_t$ (Fig. 1e–g) suggest that the model has considerable difficulty in predicting day-to-day variability of precipitation even though the seasonal mean is forecasted well (Fig. 1b–d). Note that regions of high mean observed rainfall (Fig. 1a) as well as large day-to-day variability (Supplementary fig 1), have high $RMSE_t$. Another interesting feature of $RMSE_t$ is that its magnitude increases with an increase in lead time, while its spatial pattern does not show much variations.

Next we investigate the error growth with lead time over three important domains of the tropical monsoon, viz., Tropics ($30^\circ S$ – $30^\circ N$, $0^\circ E$ – $360^\circ E$), South Asia ($10^\circ S$ – $30^\circ N$, $60^\circ E$ – $110^\circ E$), and North America (0° – $30^\circ N$, $60^\circ W$ – $130^\circ W$) in Fig. 2a. We find that the growth of $RMSE_t$ from day-1 to day-7 is of the order of 2 – 3 mm day $^{-1}$ over all the three regions. However, $RMSE_t$ of day-1 (8 – 14 mm day $^{-1}$) is much larger than its growth with lead-time. This suggests that the model is close to its own climatological

characteristic of day-to-day variations in precipitation by day-1, which does not change much with lead time. In particular, $RMSE_t$ as well as its growth are substantially higher over South Asia than over the tropics and North America. Another interesting feature of $RMSE_t$ is that regions of low $RMSE_t$ (tropics, North America) tend to saturate sooner as compared to South Asia.

Figure 2b depicts the Correlation Coefficient in time (CC_t) between TRMM rainfall and NGFS forecast for days 1, 4, and 7. CC_t is calculated as:

$$CC_t = \frac{1}{N} \sum_{i=1}^N \left[\frac{(M_i - \bar{M})(O_i - \bar{O})}{\sigma_M \sigma_O} \right], \quad (2)$$

where \bar{M} and \bar{O} represent the time-averaged model and observed precipitation, respectively and other symbols are the same as those used in Eq. 1. CC_t decreases with lead time for all three regions chosen for this study. NGFS has higher skills for the day-1 forecast over tropics and North America as compared to South Asia, but with an increase in lead time, the skill over South Asia improves in comparison to Tropics and North America. This improvement in skill over South Asia in comparison to North America primarily comes from oceanic regions (not shown). As ocean parts of South Asia have much higher skills as than compared to over North America in terms of CC_t .

To examine this high and rapid increase in error in NGFS precipitation forecasts over South Asia, we have considered this region for a detailed analysis. As South Asian monsoon shows large spatio-temporal variability in terms of intensity and phase (timing) of precipitation. Therefore, it's essential

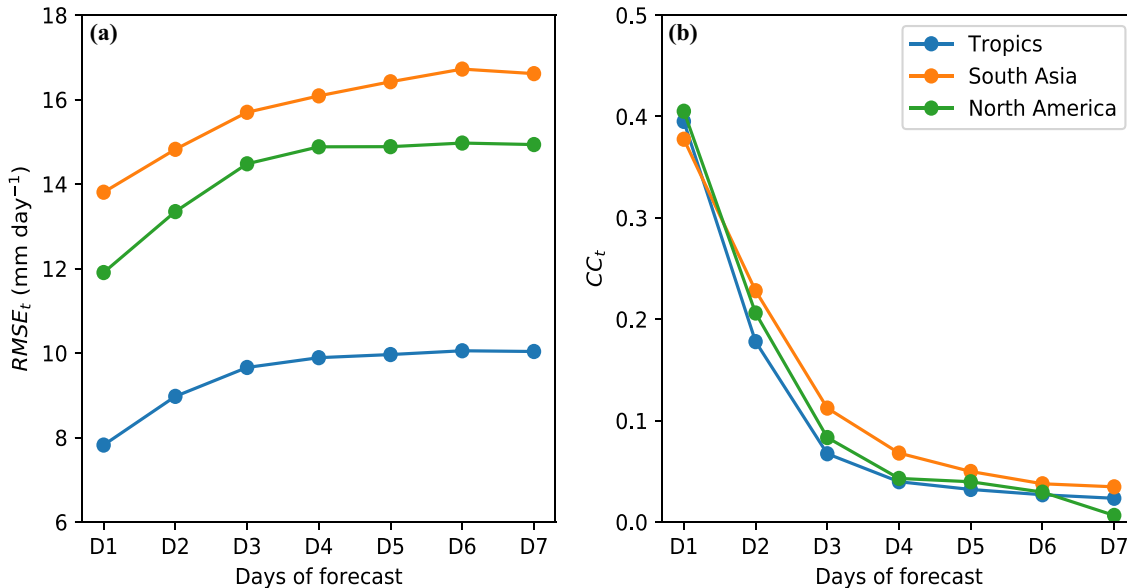


Fig. 2 Area averaged $RMSE_t$ and correlation coefficient (CC_t) of observed and model precipitation (mm day^{-1}) for 7 days lead time over the tropics ($30^\circ S$ – $30^\circ N$, $0^\circ E$ – $360^\circ E$), South Asia ($10^\circ S$ – $30^\circ N$, $60^\circ E$ – $110^\circ E$) and North America ($0^\circ E$ – $30^\circ N$, $60^\circ W$ – $130^\circ W$)

to characterize the model error both spatially as well as temporally. In this work, our primary objective is to examine the NGFS model's error characteristics based on its variability in space and time. NGFS is an atmospheric model in which land is coupled with atmosphere, but sea surface temperature is prescribed as fixed for all the days of forecast. Hence, we carry out our analysis over land and ocean separately.

4.1 Spatial variability of error

From Fig. 1, we have identified that the spatial distribution of RMSE_t is functionally dependent on observed mean precipitation and its variability. In this section, we will explore more about this relationship. How does this hold over land and ocean, and how does that change with forecast lead time?

The dependence of RMSE_t over a region on the observed mean precipitation (\bar{P}) and its day-to-day variability (measured as the daily standard deviation, \hat{P}) at the same location is shown in Fig. 3. We construct this figure by averaging RMSE_t for different ranges (bins) of \bar{P} and \hat{P} separately over the South Asian land and ocean. In general, the observed daily variations of precipitation (\hat{P}) increases with its seasonal mean (\bar{P}) both over land and ocean. However, we notice high \hat{P} ($> 35 \text{ mm day}^{-1}$) even at moderate \bar{P} ($10\text{--}20 \text{ mm day}^{-1}$) over ocean, which is absent over land. Average RMSE_t (indicated by shades) are large over regions where the \bar{P} and \hat{P} both are large (top-right corners of the shading). Over land, increase in RMSE_t with lead time is mostly confined over regions of large \bar{P} and \hat{P} . However, increase in RMSE_t over ocean is seen over regions of moderate \bar{P} with large \hat{P} . This result suggests that error growth over ocean is not only limited to regions of high \bar{P} . Similar result was obtained in Chakraborty (2010) for ECMWF model thus looks like a common feature of global forecasting models.

It is clearly understood from Fig. 3 that model forecast error has a large dependency on observed mean precipitation. This relationship is explained in more detail in Figs 4 and 5. Figure 4 represents the scatter plot between the mean observed rainfall and forecast error (RMSE_t) for days 1, 4, and 7 over South Asian land and ocean regions. Over ocean, error is more concentrated above its seasonal mean precipitation (shown by a red line) for all days of forecast. As lead time increases, it slightly drifted away from its seasonal mean rainfall. However, over land the spread of the rainfall error is much more than that of the oceanic region. This is related to the presence of high error associated with orographic rainfall over foothills of the Himalayas, Myanmar mountains, and along the Western Ghats (not shown). Similar to ocean, RMSE_t over land is also higher than its seasonal mean rainfall.

In Fig. 5, we show the upper and lower-5 percentile of error for different precipitation ranges (Fig. 4) to

demonstrate how error propagates with lead time at different precipitation range. It is observed that over ocean, upper-5 percentile error increases with lead time for every precipitation ranges, whereas lower-5 percentile error values increase for high precipitation range only. It can be inferred that error growth over ocean is mainly contributed by increase in upper-5 percentile error values, while lower-5 percentile only contributes to high precipitation. Such an increase in upper and lower-5 percentile error is limited over land, especially for the lower range of precipitation.

To examine how these errors are distributed over land and ocean, and how does it vary with lead time, we have shown the probability distribution function (PDF) of RMSE_t for days 1, 4, and 7 forecast (Fig. 6). It can be clearly seen that for the day-1 forecast, the number of grids having low error is more over ocean than land, while this behavior is opposite for larger RMSE_t . With an increase in lead time, the PDF of RMSE_t seems to be higher over ocean in comparison to land. This abrupt increase over ocean results from an increase in the number of grids having high error, thus it can be inferred that error saturates faster over ocean than land. This is also seen in Fig. 3.

4.2 Temporal variability of error

In this section, we study the error associated with temporal differences in precipitation between the model and the observation. Based on (Yang 2017), we have decomposed the total error (mean square error, MSE) into two components: MSE by mean difference (MMD) and MSE by phase variation (MPV). MMD signifies the difference in the mean intensity captured by the model and TRMM, and MPV represents the temporal shift in the model's precipitation as compared to observation. According to this formula, the total error is written as:

$$\text{MSE}^2 = \underbrace{(\bar{M} - \bar{O})^2}_{\text{Error by meandifference}} + \underbrace{(\sigma_M^2 + \sigma_O^2 - 2\sigma_M\sigma_O R)}_{\text{Error by phase variation}} \quad (3)$$

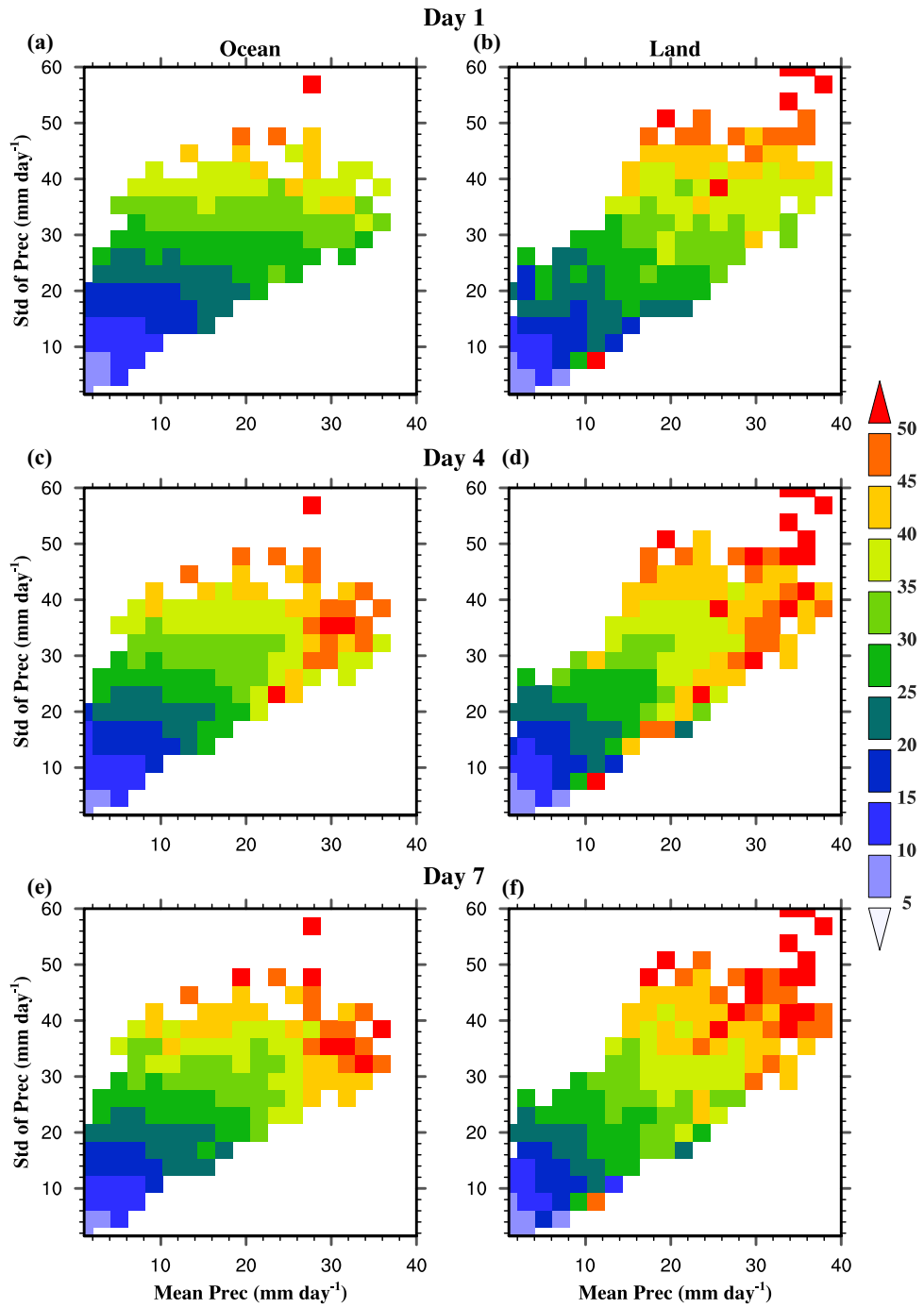
In the equation above, the variance of forecast and observation are given respectively as:

$$\sigma_M^2 = \frac{1}{N} \sum_{i=1}^N [(M_i - \bar{M})^2] \quad (4)$$

$$\sigma_O^2 = \frac{1}{N} \sum_{i=1}^N [(O_i - \bar{O})^2] \quad (5)$$

Finally, the anomalous phase correlation is written as:

Fig. 3 RMSE_t (mm day⁻¹) in precipitation forecast for days 1, 4, and 7 is represented as a function of observed mean precipitation and standard deviation over South Asian land and ocean separately



$$R = \frac{1}{N} \sum_{i=1}^N \left[\frac{(M_i - \bar{M})(O_i - \bar{O})}{\sigma_M \sigma_O} \right] \quad (6)$$

MSE and its components averaged over South Asian land and ocean for 7-days forecast are shown in Fig. 7. It is noted that total MSE and its components are higher over land than ocean for all days of forecast. Its rate of growth also shows the increasing trend over both regions, except for the day-2 forecast over land. Hence, the error growth rate (r) over

both regions are computed from day-2. The growth rate of total MSE ($r_{\text{tot-land}}: 17.9$, $r_{\text{tot-ocean}}: 11.9$) and its components ($r_{\text{MMD-land}}: 3.8$, $r_{\text{MMD-ocean}}: 0.5$ and $r_{\text{MPV-land}}: 14.1$, $r_{\text{MPV-ocean}}: 10.1$) shows that land has higher growth rate than ocean. Therefore, MSE as well as its growth is substantially higher over land than ocean. It can also be seen that more than 90% of the total error is contributed by phase (time) variation over both regions. This highlights that the model's precipitation phase is incoherent with the observation over both land and ocean.

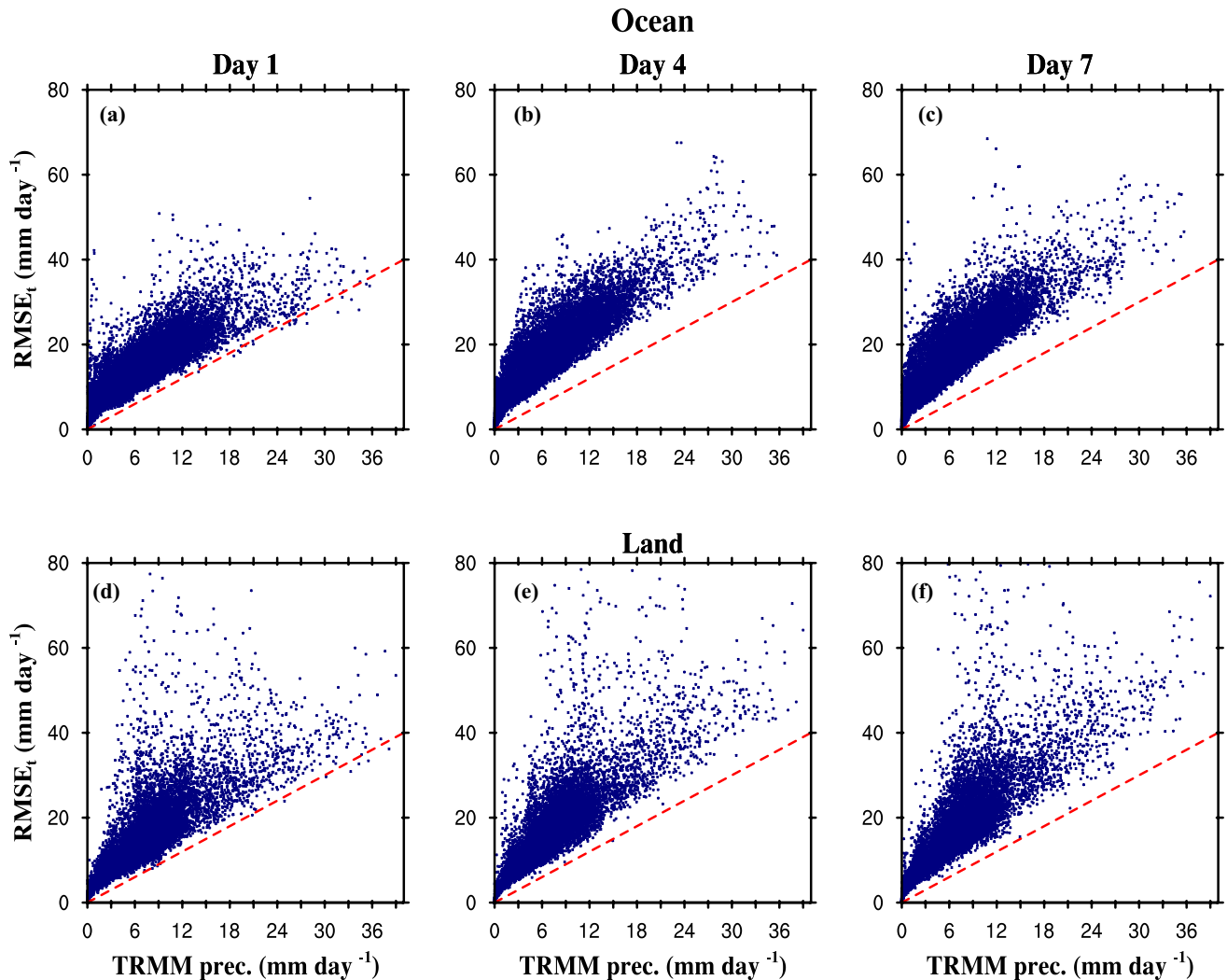


Fig. 4 Top panel shows the scatter plot between observed TRMM precipitation (mm day^{-1}) and corresponding error in NGFS precipitation over South Asian **a–c** ocean and the bottom panel shows the same over **d–f** land for days 1, 4, and 7 forecast, respectively

To investigate further about the model's skills over land and ocean, the correlation coefficient between the NGFS forecast and observed precipitation is shown in Fig. 8. We find that the model shows low skill over land in comparison to ocean till a lead time of day-5. After that, both regions behave in a similar manner. This result is consistent with the above finding (Fig. 7), suggesting that our model's performance is better over oceanic regions when compared to land. Next, we examine the causes of high forecast error over land areas than oceans.

As discussed earlier, the majority (about 90%) of the error is emanating from MSE by phase (timing) variation. South Asian monsoon exhibits large temporal variabilities ranging from subdiurnal-to-multidecadal. There is a possibility that variabilities in these timescales can lead to high error over land region. Therefore, we attempt to understand the

intraseasonal and diurnal variability components from the 7-days forecast.

4.2.1 Intraseasonal timescales

Various quasi-periodic intraseasonal variability modes (low-frequency (30–90 day) and high-frequency (10–20 day) are known to be associated with the South Asian monsoon rainfall (Dakshinamurthy and Keshavamurthy 1976; Yasunari 1979; Sikka and Gadgil 1980; Krishnamurti and Ardanuy 1980; Chen and Chen 1993). As intra-seasonal variability over Indian region can be understood as a superposition of phases of high- and low-frequency oscillations (Karmakar et al. 2017). We investigate the strength of these variabilities by band-passing the rainfall time series of 116 days. We take rainfall over central India

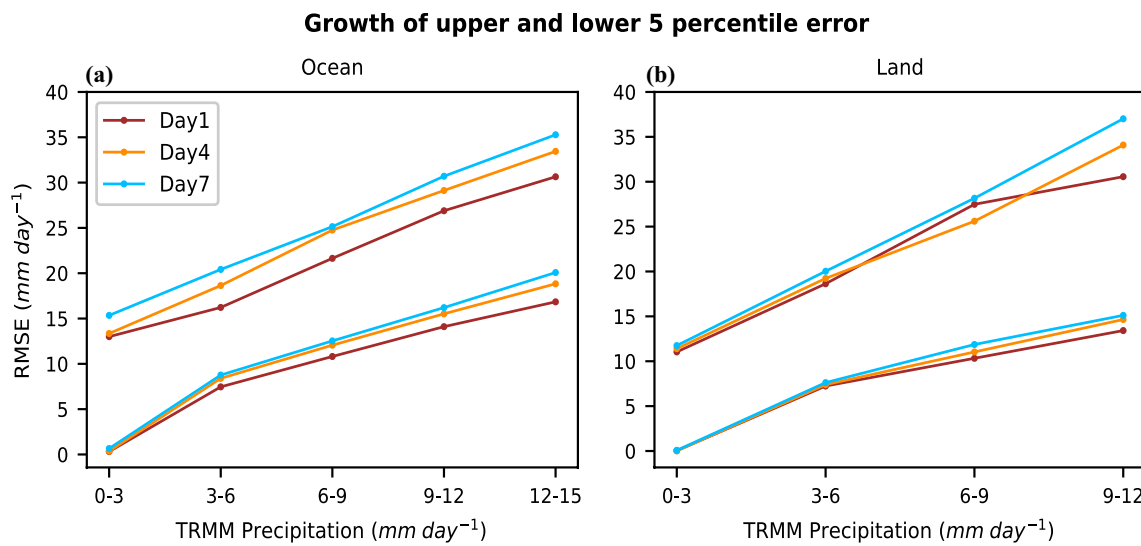


Fig. 5 Upper and lower 5 percentile error values over the range of TRMM precipitation over South Asian **a** ocean, **b** land for days 1, 4, and 7 forecast

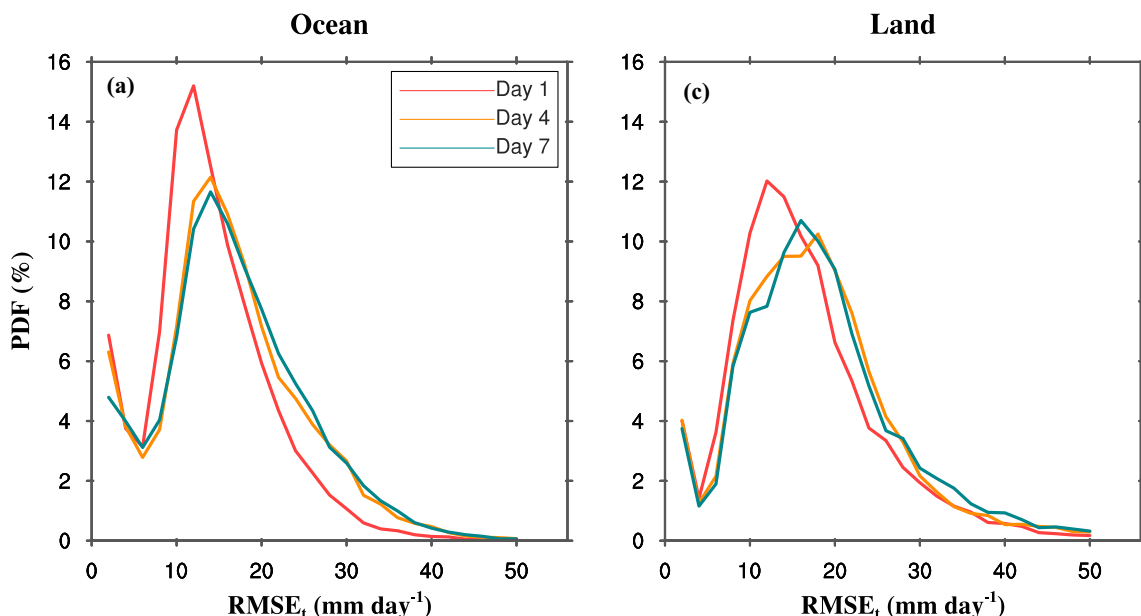


Fig. 6 Probability distribution function (PDF) of RMSE_t for days 1, 4, and 7 forecasts over the South Asian **a** ocean and **b** land region

(16.5° N– 26.5° N, 74.5° E– 86.5° E) to be the representative of the South Asian land region and analyze intraseasonal variability patterns.

Figure 9a shows the daily mean area-averaged rainfall from TRMM and NGFS forecast for days 1, 4, and 7 over central India. We find that the day-1 forecast reasonably captured the overall transition between wet and dry spells of precipitation. With lead time, however, the model shows considerable difficulty in capturing these extremes. For instance, day-4 and day-7 forecasts overestimated the long,

intense break from 22 June–2 July and underestimated the heavy rainfall event from (5 Sep.–9 Sep.).

We have shown the high-frequency (10–20 day) and low-frequency (30–60 day) variability in Fig. 9b–c. It is observed that for high-frequency mode, TRMM exhibits large fluctuations in June, July, and August in comparison to September. These fluctuations are captured well by the model. However, there exists a large phase error with lead time. For low-frequency mode, observation shows large variability in August and September. These variabilities are represented

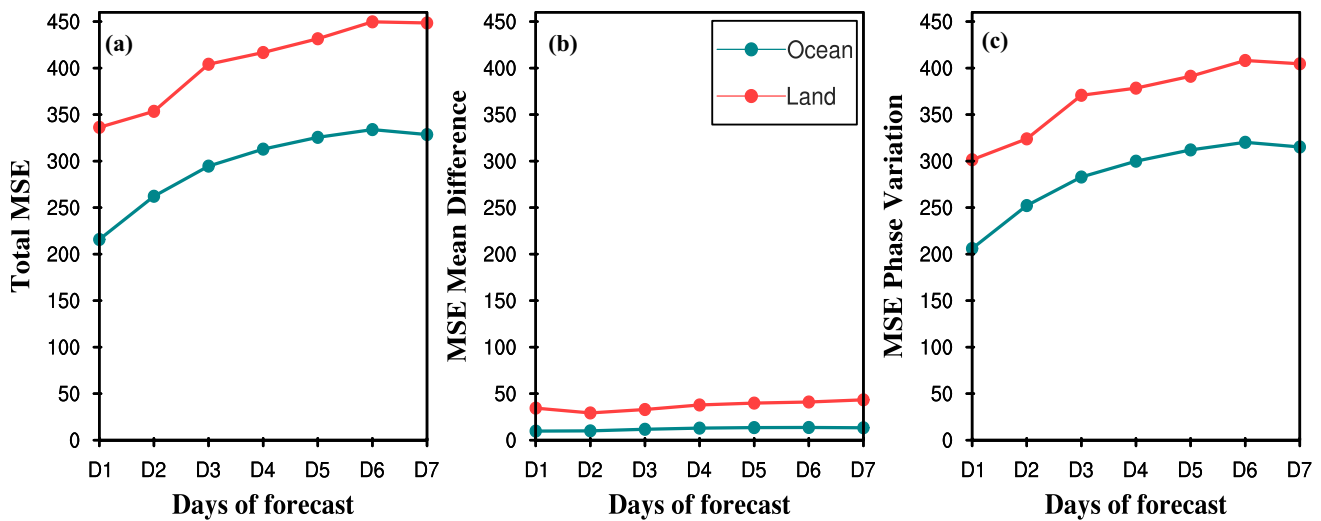


Fig. 7 **a** Total Mean square error (MSE) in NGFS forecast and its components in **b** MSE by mean difference, **c** MSE by phase variation for all days of forecast over South Asian land and ocean. Units: $\text{mm}^2 \text{ day}^{-2}$

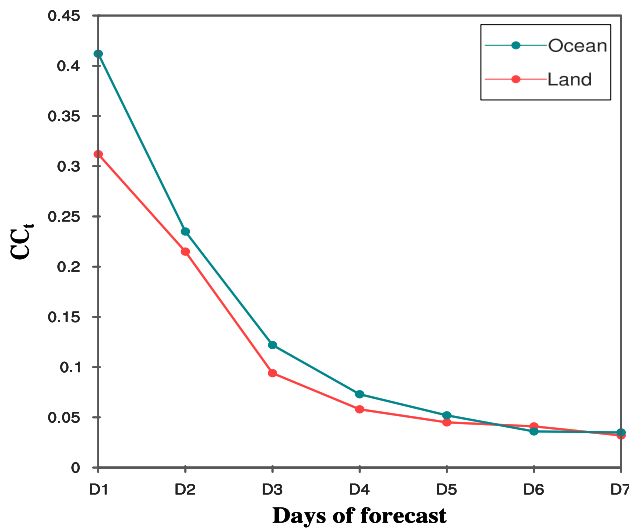


Fig. 8 Correlation coefficient in time (CC_t) between observation and model precipitation for all days of forecast over South Asian land and ocean

reasonably well by the model except for day-4, which depicts an out of phase relationship with TRMM. In order to evaluate the skill of the model in capturing these variabilities, the correlation coefficient is computed.

The first bar plot in Fig. 10 represents the correlation coefficient (CC) between the daily mean observed and model precipitation (Fig. 9a) averaged over central India. We find that CC is high for day-1 and day-2, minimum for day-4 and again increases with lead time. The reason for this peculiar behavior can be understood by examining the model's ability to capture the different modes of variability embedded in the monsoon system. These variabilities include synoptic

disturbances (< 10 day), high-frequency (10–20 day), and low-frequency (30–60 day) modes. The CC of these variabilities between filtered TRMM and NGFS precipitation is represented in the other bar plots in Fig. 10. For the day-1 and day-2 forecast, CC is positive for all the three modes. This suggests that all these modes of variability are in phase with the observation. Thus, NGFS's skills are highest for a shorter lead time. Day-4 forecast shows out of phase relationship (CC negative) for synoptic disturbances and low-frequency mode. This may be the reason for the minimum skill of the NGFS model for the day-4 forecast. With lead time, the performance of the model improves as compared to the day-4 forecast. This is due to the high positive CC of low-frequency mode. It can be inferred that low-frequency mode and synoptic disturbances largely govern the performance of the model over this region.

Figure 11 shows the probability distribution function of precipitation over central India from TRMM and NGFS forecast for days 1, 4, and 7. It can be seen that observation shows a bimodal peak at around 3 mm day^{-1} (dry phase) and $7\text{--}12 \text{ mm day}^{-1}$ (wet phase). This distribution is depicted reasonably well by the day-1 forecast of the model. With increasing lead time model has, however, high tendency to predict the dry phase of precipitation over this region.

4.2.2 Diurnal timescales

From previous studies, it is known that error in the diurnal timescales can accumulate in the intraseasonal and seasonal time scales and can get reflected in the total error (Slingo et al. 2003; Chakraborty 2010). Chakraborty and Krishnamurti (2008) showed that the kinetic energy of the diurnal timescale contributes to the total energy of monsoon

Fig. 9 **a** Intraseasonal variability of precipitation from observation and model **b** 10–20 day propagation mode. **c** 30–60 day propagation mode of the intra-seasonal variability of Indian monsoon averaged over central India (16.5° N– 26.5° N, 74.5° E– 86.5° E) for days 1, 4, and 7 forecast

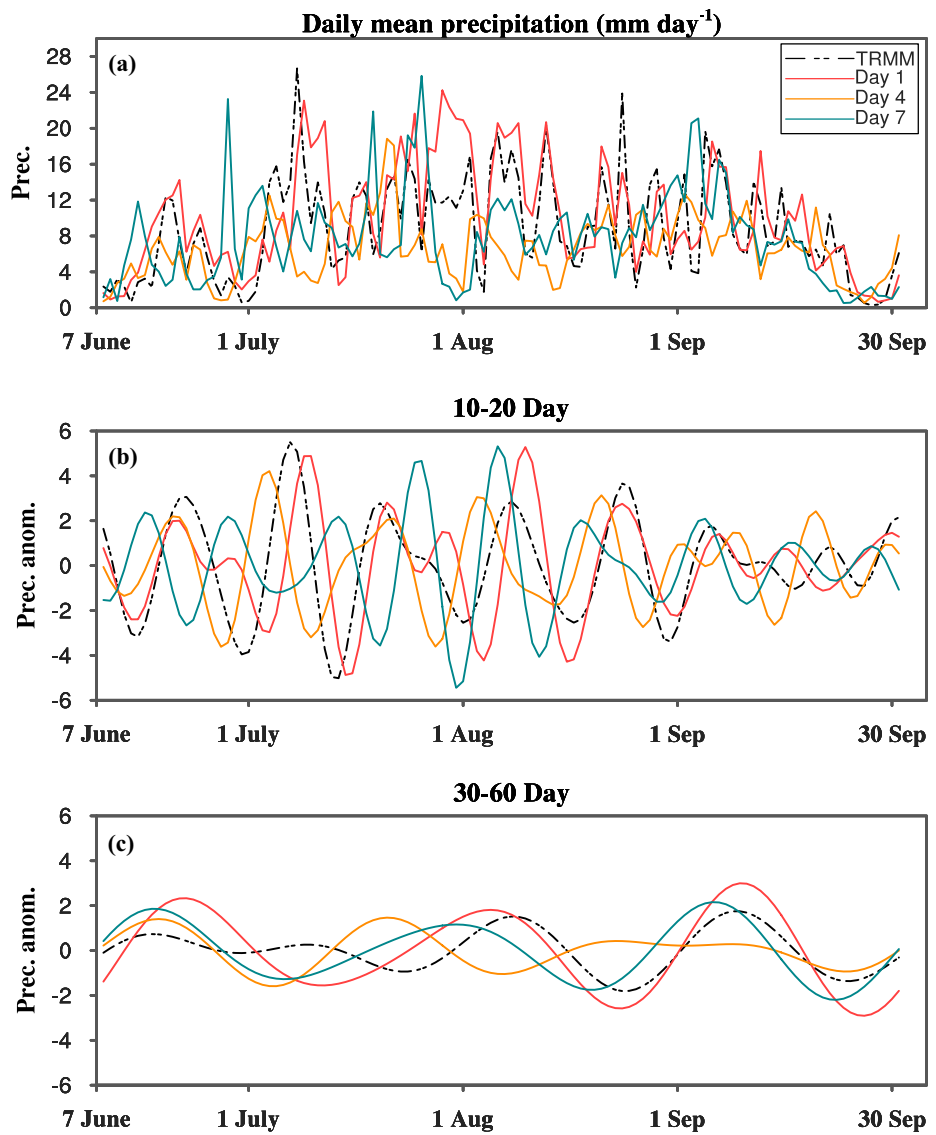
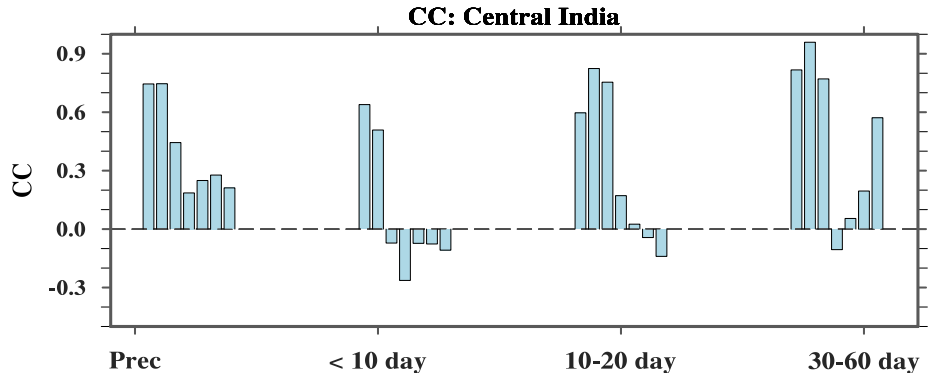


Fig. 10 Correlation coefficient (CC) of daily mean observed and model precipitation, synoptic variability (< 10 day), 10–20 and 30–60 day modes of the intra-seasonal variability of Indian monsoon averaged over central India (16.5° N– 26.5° N, 74.5° E– 86.5° E) for all days of forecast



circulation. Here we consider studying the behavior of the NGFS model in capturing diurnal variability of precipitation over the South Asian region for JJAS. We have used 3 hourly output from TRMM estimates and NGFS model.

The diurnal component is extracted by using Fast Fourier Transform (FFT) on the time-series of octet of precipitation for each day. The first harmonics of the transformed series represents the diurnal cycle. The average of hour-by-hour of

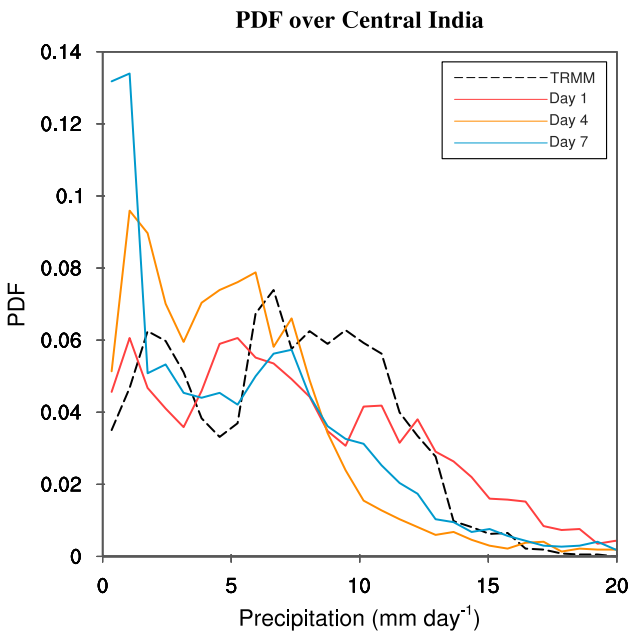


Fig. 11 Probability density function (PDF) of the seasonal mean precipitation from observation and model for days 1, 4, 7 forecast over central India (16.5° N– 26.5° N, 74.5° E– 86.5° E)

the first harmonics of the filtered data resulted in the diurnal cycle for the entire period of forecast. The maximum value corresponds to the amplitude and hour at which maxima occurs represents the phase of the diurnal cycle.

The geographical distribution of the amplitude of the diurnal cycle from both observation and model over the South Asian region is shown in Fig. 12. Figure 13 shows the same for the phase of the diurnal cycle. It can be clearly seen that model forecast at days 1, 4, and 7 show striking resemblance with the observation over northeastern Indian land, adjoining countries, and head Bay of Bengal. Despite having a patchy rainfall pattern arising due to the scaling of the gravity waves associated with orography, the model faithfully captures the intensity and spatial distribution of the amplitude. However, Fig. 13 shows that there is a phase shift of around 6-h over land for all days of the forecast. This suggests that NGFS shows early convection over land as compared to TRMM. On the other hand, parts of the ocean such as north Bay of Bengal show a phase error of around 3-h, while the phase is captured well by the model over south Bay of Bengal.

Further, we illustrate the phase and amplitude of the diurnal cycle with lead time over central India between observation and model forecast for days 1, 4, and 7 (Fig. 14). A 6-h time-lag in the maxima of rainfall between the observation

Fig. 12 Amplitude of the diurnal **a** TRMM observed rainfall estimates and those produced by the NGFS model for days 1, 4, and 7 forecast **b–d** over the South Asian region. Units: mm day^{-1}

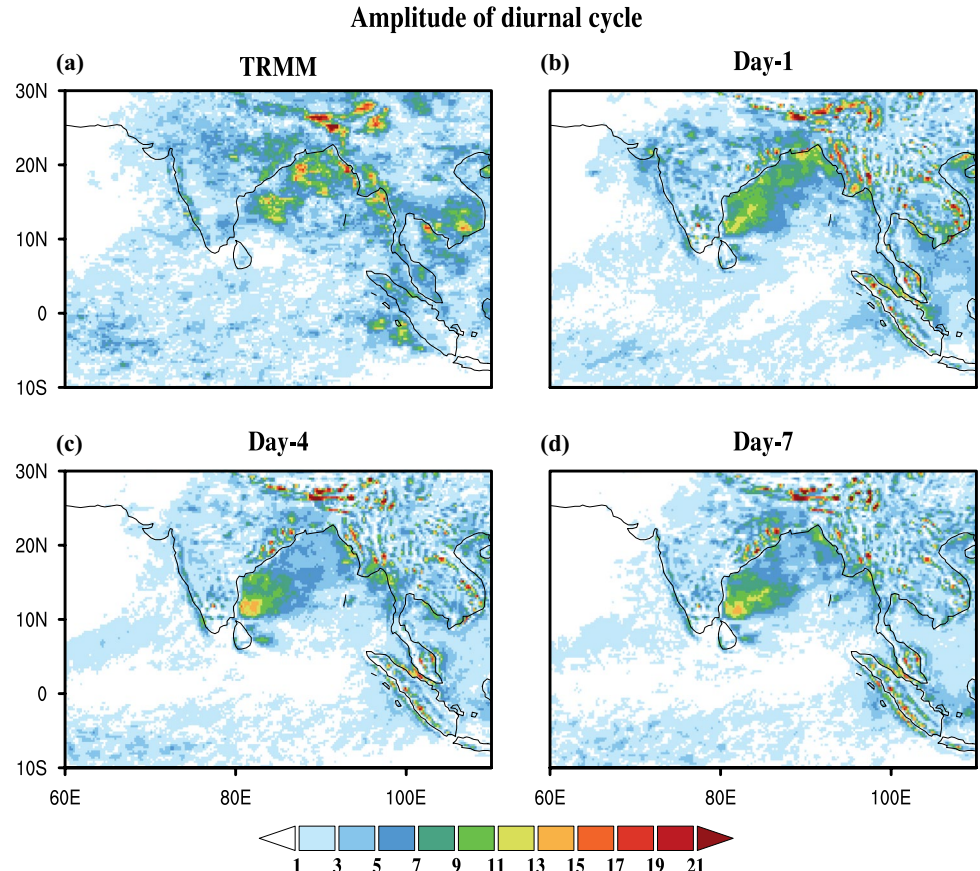


Fig. 13 Phase of the diurnal a TRMM-observed rainfall estimates and those produced by the NGFS model for days 1, 4, and 7 forecast b–d over the South Asian region. Phase angles are shown as time of the day (i.e., 0, 3, 6, 9...,21 GMT)

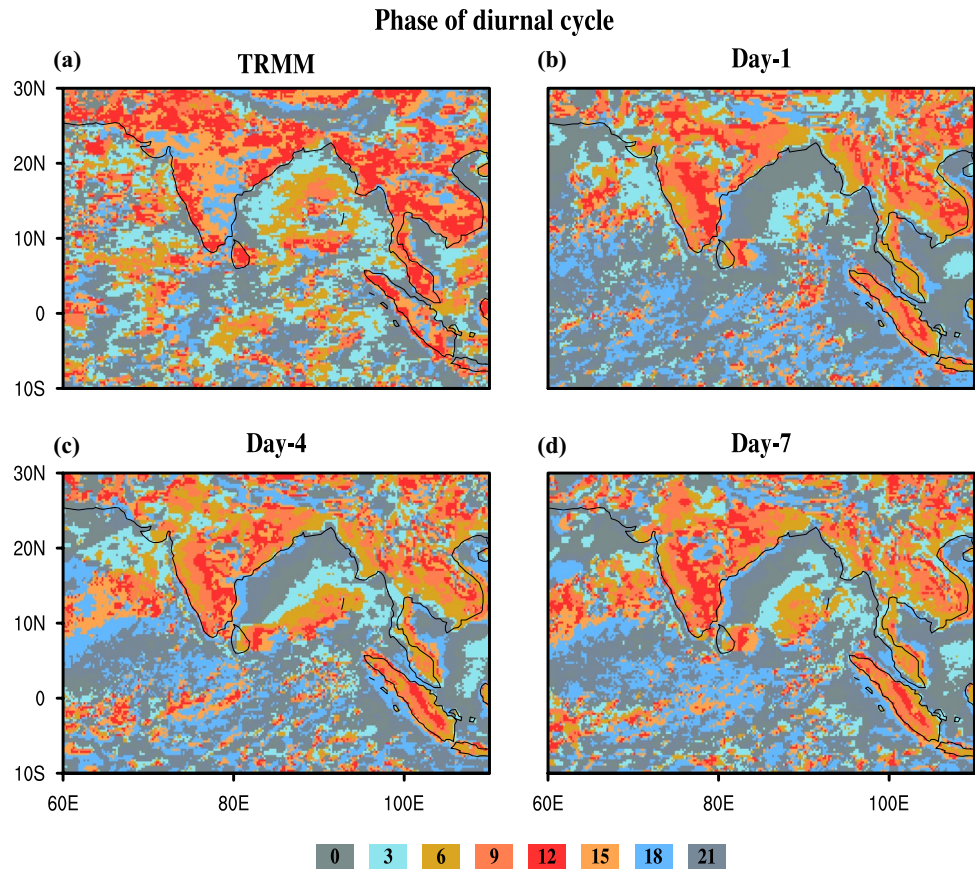
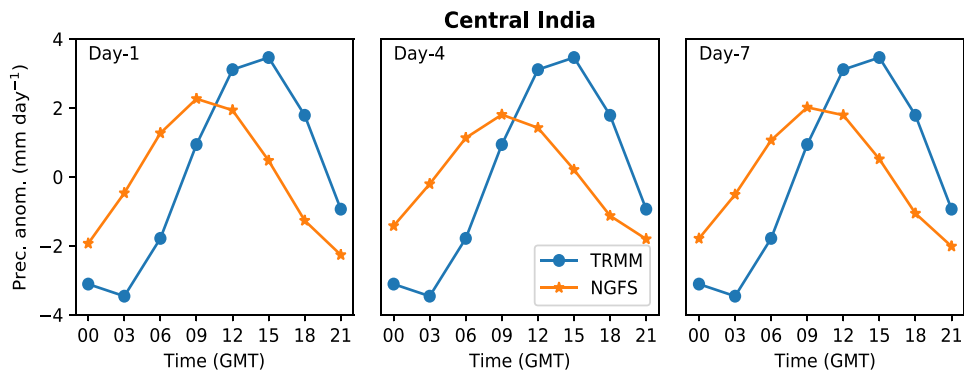


Fig. 14 The diurnal cycle of precipitation from the TRMM rainfall estimates, and from the model for days 1, 4, and 7 forecast over central India (16.5° N– 26.5° N, 74.5° E– 86.5° E)

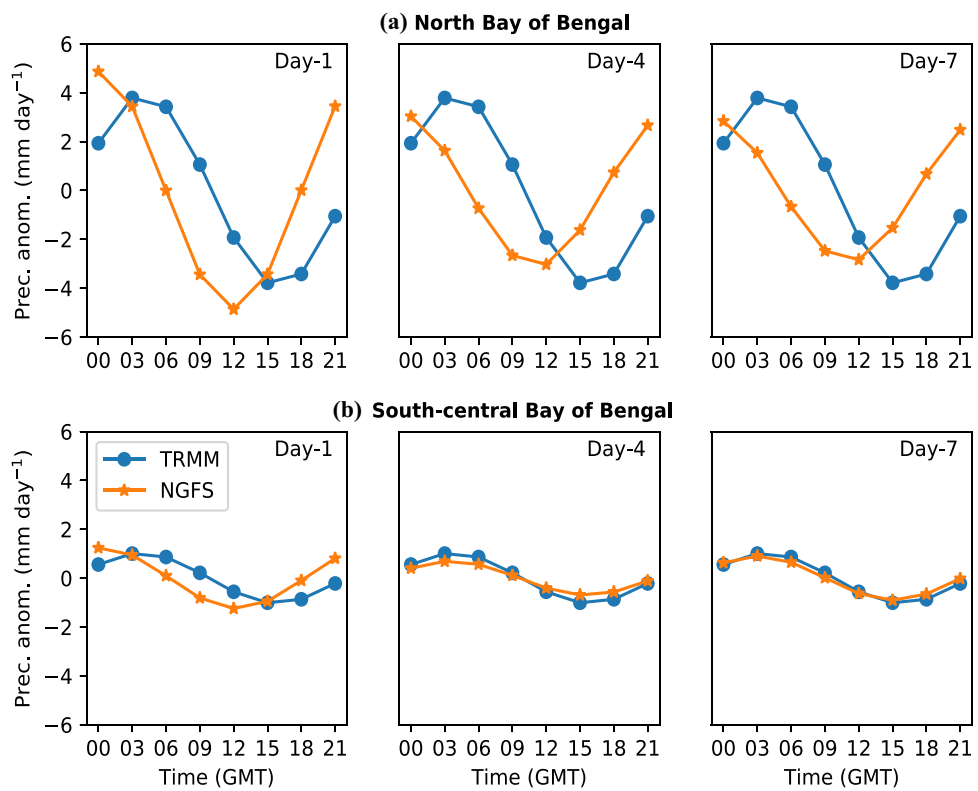


and model is evident, indicating early convection in the model. Moreover, this lag remains constant for all days of forecast and doesn't change in time. This signifies that phase error in the diurnal cycle acts just like a systematic bias in the model, while the error in the intraseasonal timescales (low-frequency mode and synoptic disturbances) govern the model error over this region.

In the South Asian oceanic region, north Bay of Bengal (12° N– 24° N, 70° E– 90° E) and south-central Bay of Bengal (5° N– 12° N, 85° E– 95° E) show large diurnal variability (Figs. 12, 13). Hence, these regions are considered to analyze the phase and amplitude of the diurnal cycle over ocean

(Fig. 15). Over north Bay of Bengal (BoB), observation shows maxima at 03 GMT, whereas the model has a peak at 00 GMT for all days of forecast. This suggests a 3-h phase error over North BoB. Over South BoB, the model captures both the phase and amplitude of the diurnal cycle reasonably well. Over ocean, the amplitude and phase of the diurnal cycle do not change much with lead time.

Fig. 15 The diurnal cycle of precipitation from the TRMM rainfall estimates, and from the model for days 1, 4, and 7 forecast over **a** north Bay of Bengal (12° N– 24° N, 70° E– 90° E) and **b** south-central Bay of Bengal (5° N– 12° N, 85° E– 95° E)



4.3 Comparison between daily and diurnal timescales

In the previous sections, we have characterized the error of the NGFS model at different timescales over South Asian land and ocean separately. Errors arising from smaller timescales can get reflected in the error of the seasonally forecasted variable (Colle et al. 2001). Therefore, it is important to notice the resemblance between their characteristics at various time periods. This section outlines the similarities and differences in the error characteristics at daily and diurnal timescales.

Figure 16 shows the spatial distribution of the seasonal mean precipitation at every alternate 3-h of the day from TRMM (Fig. 16a–d) and NGFS day-1 forecast (Fig. 16e–h) over the South Asian region. Convection is active over ocean during 00 and 06 GMT in observation, whereas the model precipitates at all times of the day, especially over north Bay of Bengal. This leads to high error over this region. TRMM shows active convection over land during 18 and 24 GMT, while model shows during 12 and 18 GMT. Moreover, the model rains throughout the day along the foothills of the Himalayas. The bottom panel represents RMSE_t calculated between TRMM and model day-1 forecast. The model shows large error over most parts of the South Asian region such as north Bay of Bengal, equatorial Indian ocean, central India, and the Western Ghats. The main difference between the daily (Fig. 1e) and diurnal timescales is that model error

increased substantially at the diurnal timescales. To understand the reason, we have applied the error decomposition method discussed in the previous section.

Total MSE and percentage contribution from its 2 components at an interval of 3-h over South Asian land and ocean are shown in Fig. 17a, b and c, d, respectively. As can be seen from the figure that total error over ocean peaks at around 03 GMT and has minimum at 12 GMT. On the other hand, the error is maximum (minimum) at 12 GMT (06 GMT) over land. Thus, error over land and ocean peaks at different hours of the day. Similar to the error at daily timescales, day-1 forecast error is higher as compared to its error growth with lead time. Although MSE values are higher, there is not much change in the error with lead time over both land and ocean. Its component analysis suggests that MSE by phase variation contributes to more than 90% over both land and ocean as compared to MSE by mean difference. This result is the same as that at the daily timescales. It is interesting to note that the contribution of MSE by phase variation is more over ocean, whereas the contribution of MSE by mean difference dominates over land.

The spatial distribution of error growth rate computed over the same domain for daily and diurnal (00, 06, 09, and 18 GMT) timescales are shown in Figs. 18 and 19. We find that the error growth rate is zonally asymmetric over the Indian region i.e., error growth rate decreases over northwest India while increases over central India. This can be seen in diurnal timescales, as well (Fig. 19). The error

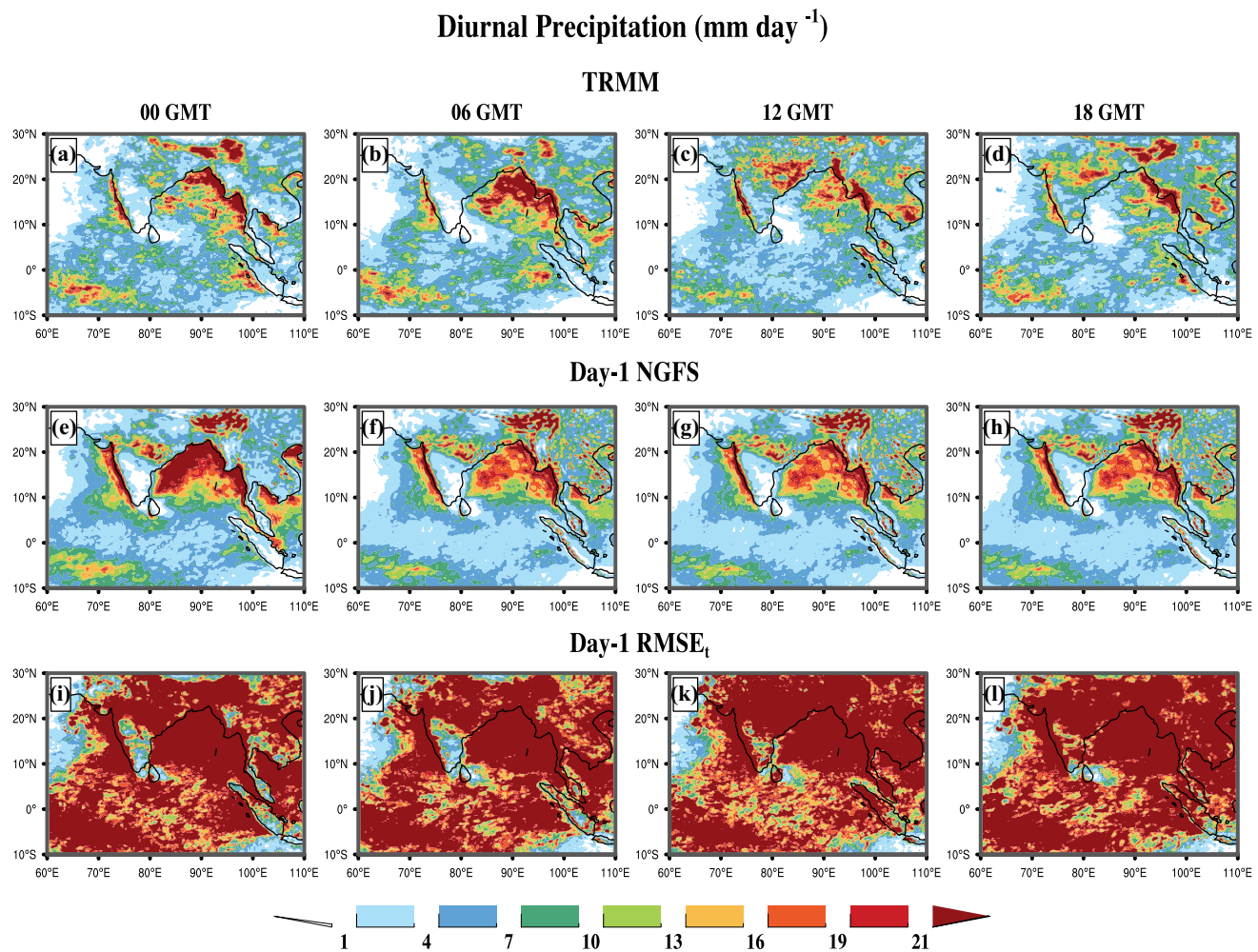


Fig. 16 Seasonal mean precipitation (mm day^{-1}) at every alternate 3-h interval (00 GMT, 06 GMT, 12 GMT, 18 GMT) over South Asian region from **a–d** TRMM observation, **e–h** NGFS day 1 forecast, **i–l** RMS Error in time for the same period

growth rate is, however positive over most parts of the oceanic region except the coast of Gujarat in both daily and diurnal timescales.

4.4 Robustness of the NGFS error characteristics for different years

To examine the robustness of error characteristics of NGFS, we have compared our results for 2012 with 2013 (Fig. 20). Indian summer monsoon rainfall (ISMR) anomaly was 6.3% below its long-term mean (1951–2015) in 2012. In the following year 2013, ISMR was 13% above its long-term mean. Hence, analyses for these 2 years: one below and another above long-term average will provide more comprehensive understanding of the error characteristics.

In this section, we have validated 3 important conclusions drawn from the forecast for 2012 with that for 2013. Figure 20a shows the Mean square error (MSE) resulting from phase and intensity averaged for all days of forecast over the

South Asian region. It suggests that error characteristics for 2013 are qualitatively similar to 2012. For instance, error is higher over land in comparison to ocean and major part of the error (about 90%) arises from the model's inability to capture the correct phase of precipitation.

We also find that the skill in predicting synoptic disturbances (< 10 day) in 2013 is reasonably high only for day-1 and day-2 after which there is a large drop in skill. This confirms that NGFS has inherent difficulty in capturing these variations after day-2 forecast. Like 2012, both high-frequency (10–20 day) and low-frequency (30–60 day) intraseasonal oscillations for 2013 are reasonably captured up to day-3 by the model. Hence, suggesting that NGFS prediction skills at intraseasonal timescales remains similar from one year to the other.

We have compared phase and amplitude of the diurnal cycle of precipitation over central India for 2012 with 2013 (Fig. 20c). We find that similar to 2012, model shows precipitation maxima at 09 GMT for 2013. Moreover, the

Fig. 17 **a, b** Total mean square error (MSE) in NGFS forecast for all 7-days forecast and its components (**c** MSE by mean difference and **d** MSE by pattern variation) percentage contribution averaged for all lead time at every 3-h of the day over South Asian land and ocean separately

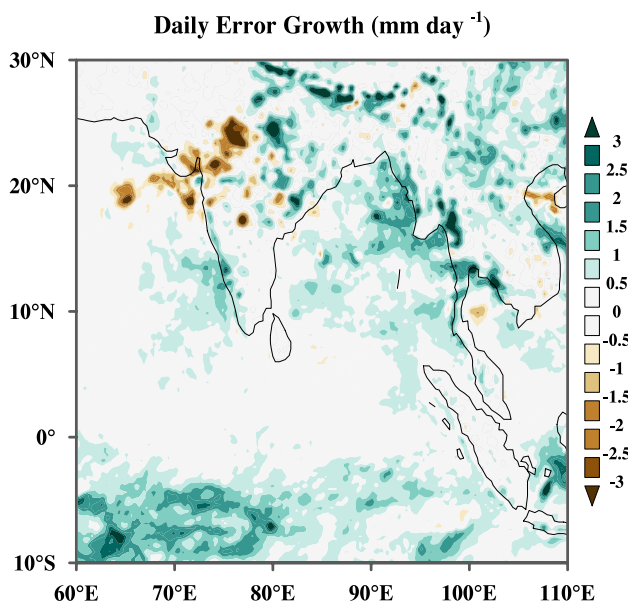
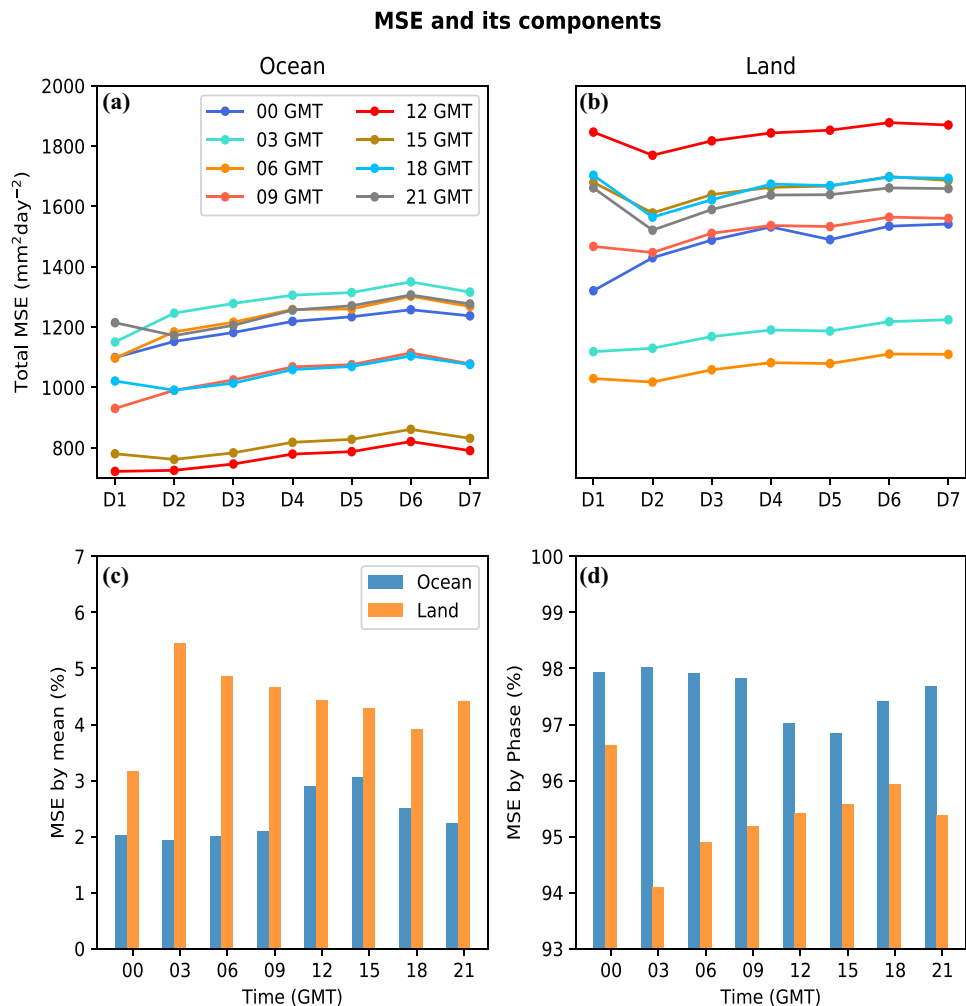


Fig. 18 Spatial distribution of error growth rate of precipitation forecast from day-1 to day-7 at daily timescales over the South Asian region

amplitude of the diurnal cycle also remains nearly same during both the years. Thus, we have demonstrated that the error characteristics of NGFS are independent of the seasonal mean rainfall.

5 Conclusions

The spatio-temporal variability in the intensity and frequency of South Asian monsoon has significant socio-economic impacts. Hence, understanding the error characteristics arising from these variabilities can eventually help in improving the prediction of the monsoon rainfall, which is essential for various sectors like hydrology, agriculture, and disaster preparedness. Under the National monsoon mission, NGFS is identified as a potential forecast system for the Indian summer monsoon. Therefore, it is important to address the fidelity of precipitation forecast made by NGFS. In this study, we have characterized its error both spatially and temporally over South Asian land and ocean

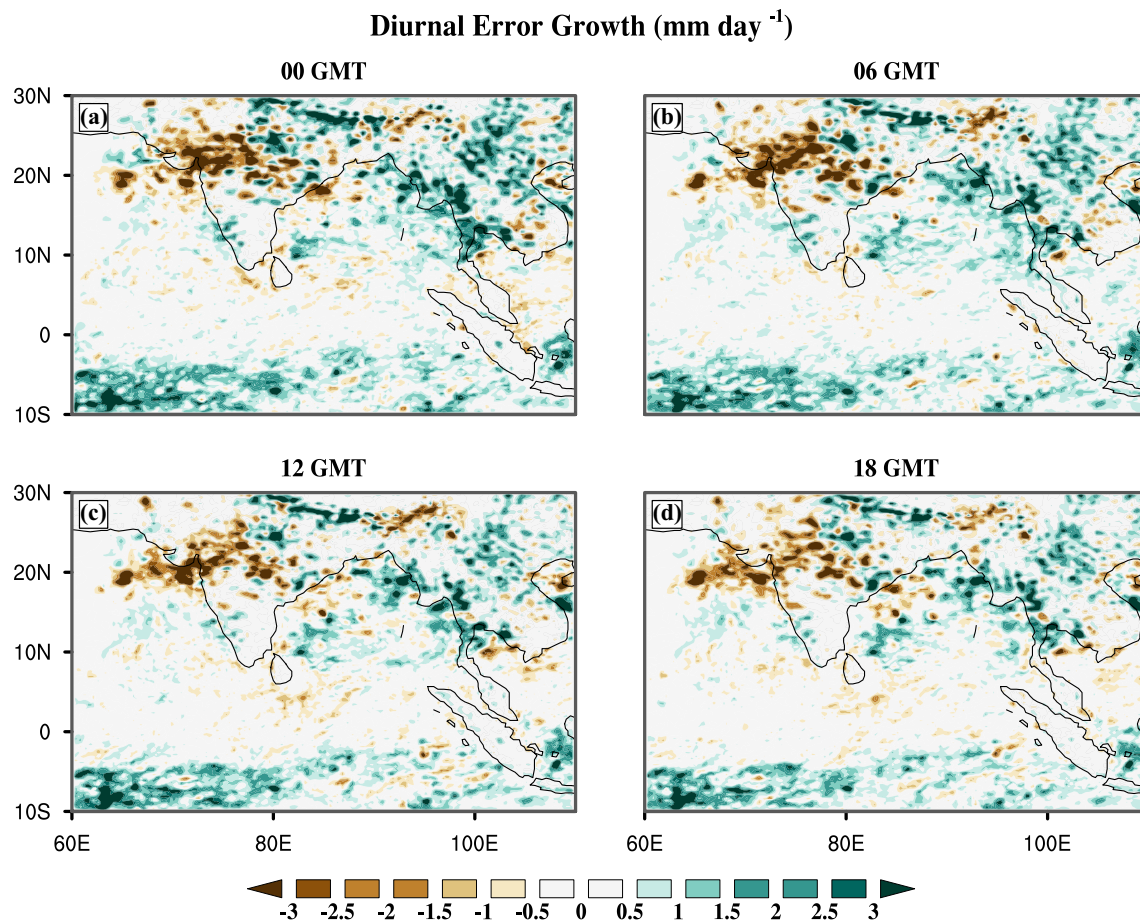


Fig. 19 Spatial distribution of error growth rate of precipitation forecast from day-1 to day-7 at every alternate 3-h (00 GMT, 06 GMT, 12 GMT, 18 GMT) over the South Asian region

separately for the boreal summer season of 2012 and validated important conclusions with the 2013 forecast.

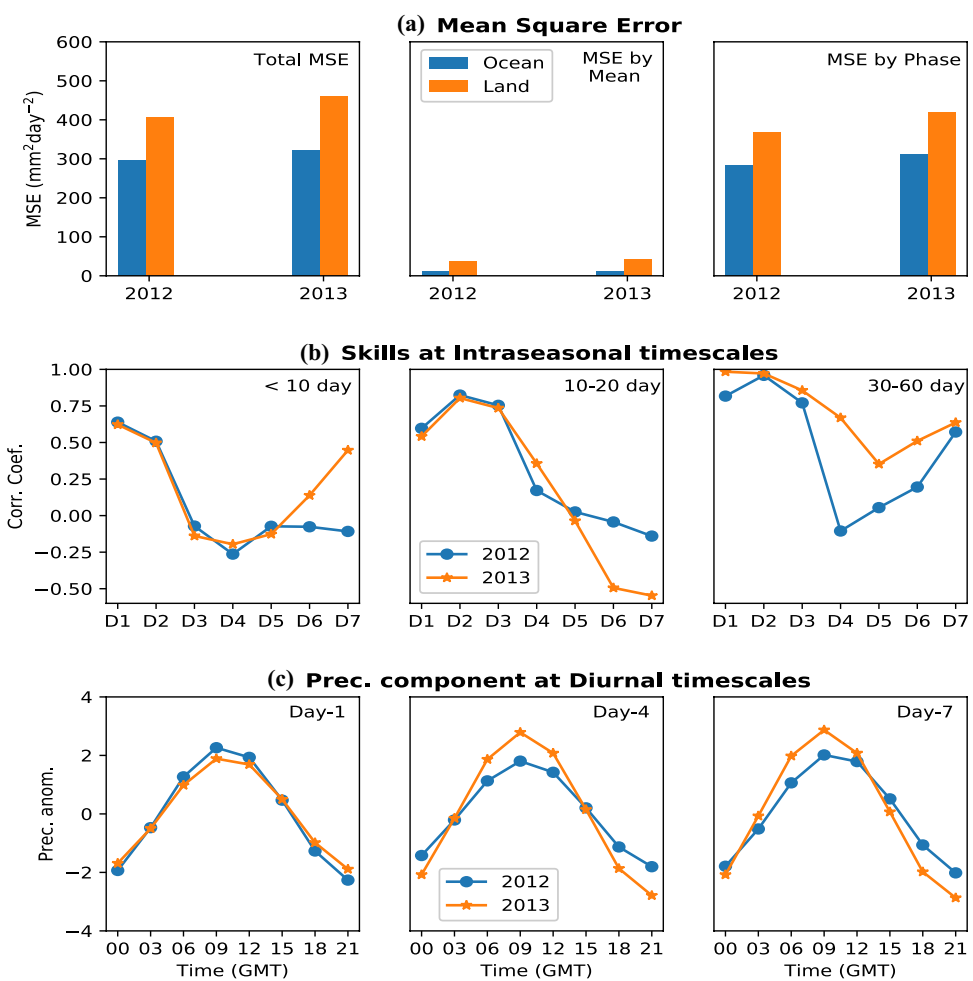
The major results are summarized as follows:

- Even though NGFS captures overall seasonal mean precipitation reasonably well, it has considerable difficulty in capturing large day-to-day fluctuations. To investigate how error grows with lead time, 3 important regions (Tropics, South Asia, and North America) of global monsoon are selected. We found that day-1 forecast error ($8\text{--}14 \text{ mm day}^{-1}$) is substantially higher than its respective error growth ($2\text{--}3 \text{ mm day}^{-1}$) for all 3 regions. This suggests that most of the error in the model accumulates within the first 24-h of the forecast. In all 3 regions, saturation error is about 15–25% and saturates within 3–5 days of forecast initiation. Over South Asia, RMSE_t and its growth rate are higher as compared to tropics and North America, but the model shows improved skills with lead time over this region. This improvement in skills primarily comes from the oceanic regions. To understand this peculiar behavior

of NGFS over South Asia, we have considered this region.

- Spatial analysis of error suggests that over oceanic regions, high error is primarily confined to a region of large day-to-day variability. In contrast, over land it is mainly present at locations of high mean precipitation. With lead time error grows faster over grids where both observed mean precipitation and its variability are high. This is true over both land and ocean. The increase in error over ocean is due to an increase in the number of grids having high error, while such an increase of high error is limited over land.
- Error decomposition analysis shows that error as well as its growth is higher over land than ocean, and the majority (about 90%) of the error arises from the model's inability to capture the phase of the precipitation at various timescales. The NGFS model over land (central India) cannot capture synoptic scale variations (< 10 day) after day-2. Both the high-frequency (10–20 day) and low-frequency (30–60 day) intraseasonal variations are reasonably predicted up to day-3. The skill of the

Fig. 20 Comparison of error characteristics for 2012 with 2013. **a** MSE analysis over South Asia, **b** skill (correlation coefficient) at Intraseasonal timescales, **c** diurnal cycle of precipitation from the model for days 1, 4, and 7 forecast over central India (16.5° N– 26.5° N, 74.5° E– 86.5° E)



NGFS over this region is largely governed by its ability to capture the low-frequency mode and synoptic disturbances. At diurnal timescales, the model forecasts show a peak in precipitation about 3–6 h before that in the observed, both over land and ocean. Surprisingly, this error does not increase with lead-day of forecast.

Major conclusions of our work, based on the forecast for year 2012, have been further validated for 2013. We find that error behavior remains similar for both the years, irrespective of the fact that the ISMR anomaly is negative in 2012 (6.3% below its long-term average) and positive in 2013 (13% above its long-term average). Hence, we conclude that these forecasting errors are an inherent characteristic of the model. The source of these errors could be related to a fundamental lacuna in the model such as physical parameterization that remains to be addressed in future studies.

Acknowledgements PS thank G. Srivastava, C. Jalihal and J. B. Samuel for useful discussions. AC acknowledges the National Monsoon Mission, Ministry of Earth Sciences (MoES), Government of India for the funding this research.

References

- Anthes RA (1983) Regional models of the atmosphere in middle latitudes. *Mon Weather Rev* 111(6):1306–1335
- Beljaars AC, Viterbo P, Miller MJ, Betts AK (1996) The anomalous rainfall over the United States during July 1993: sensitivity to land surface parameterization and soil moisture anomalies. *Mon Weather Rev* 124(3):362–383. [https://doi.org/10.1175/1520-0493\(1996\)124<0362:TAROTU>2.0.CO;2](https://doi.org/10.1175/1520-0493(1996)124<0362:TAROTU>2.0.CO;2)
- Chakraborty A (2010) The skill of ECMWF medium-range forecasts during the year of tropical convection 2008. *Mon Weather Rev* 138(10):3787–3805. <https://doi.org/10.1175/2010MWR3217.1>
- Chakraborty A, Krishnamurti T (2008) Improved forecasts of the diurnal cycle in the tropics using multiple global models. Part II: Asian summer monsoon. *J Clim* 21(16):4045–4067. <https://doi.org/10.1175/2008JCLI2107.1>
- Chakraborty A, Krishnamurti T, Gnanaseelan C (2007) Prediction of the diurnal cycle using a multimodel superensemble. Part II: cloud. *Mon Weather Rev* 135(12):4097–4116. <https://doi.org/10.1175/2007MWR2080.1>
- Chen TC, Chen JM (1993) The 10–20-day mode of the 1979 Indian monsoon: Its relation with the time variation of monsoon rainfall. *Mon Weather Rev* 121(9):2465–2482. [https://doi.org/10.1175/1520-0493\(1993\)121<2465:TDMOTI>2.0.CO;2](https://doi.org/10.1175/1520-0493(1993)121<2465:TDMOTI>2.0.CO;2)
- Colle BA, Mass CF, Ovens D (2001) Evaluation of the timing and strength of MM5 and Eta surface trough passages over the

- eastern Pacific. *Weather Forecast* 16(5):553–572. [https://doi.org/10.1175/1520-0434\(2001\)016<0553:EOTTAS>2.0.CO;2](https://doi.org/10.1175/1520-0434(2001)016<0553:EOTTAS>2.0.CO;2)
- Dakshinamurthy J, Keshavamurthy R (1976) On oscillations of period around one month in the Indian summer monsoon. *Indian J Meteor Geophys* 27:201–203
- Ebert EE, Gallus WA Jr (2009) Toward better understanding of the contiguous rain area (CRA) method for spatial forecast verification. *Weather Forecast* 24(5):1401–1415. <https://doi.org/10.1175/2009WAF222252.1>
- Ebert E, McBride J (2000) Verification of precipitation in weather systems: determination of systematic errors. *J Hydrol* 239(1–4):179–202. [https://doi.org/10.1016/S0022-1694\(00\)00343-7](https://doi.org/10.1016/S0022-1694(00)00343-7)
- Fu X, Wang B, Li T (2002) Impacts of air-sea coupling on the simulation of mean Asian summer monsoon in the ECHAM4 model. *Mon Weather Rev* 130(12):2889–2904. [https://doi.org/10.1175/1520-0493\(2002\)130<2889:IOASCO>2.0.CO;2](https://doi.org/10.1175/1520-0493(2002)130<2889:IOASCO>2.0.CO;2)
- Fu X, Yang B, Bao Q, Wang B (2008) Sea surface temperature feedback extends the predictability of tropical intraseasonal oscillation. *Mon Weather Rev* 136(2):577–597. <https://doi.org/10.1175/2007MWR2172.1>
- Gadgil S, Srinivasan J (2012) Monsoon prediction: are dynamical models getting better than statistical models? *Curr Sci* 103(3):257–259
- Gadgil S, Rajeevan M, Nanjundiah R (2005) Monsoon prediction—why yet another failure? *Curr Sci* 88(9):1389–1400
- Gilleland E, Ahijevych D, Brown BG, Casati B, Ebert EE (2009) Intercomparison of spatial forecast verification methods. *Weather Forecast* 24(5):1416–1430. <https://doi.org/10.1175/2009WAF222269.1>
- Harper K, Uccellini LW, Kalnay E, Carey K, Morone L (2007) 50th anniversary of operational numerical weather prediction. *Bull Am Meteorol Soc* 88(5):639–650. <https://doi.org/10.1175/BAMS-88-5-639>
- Huffman GJ, Bolvin DT, Nelkin EJ, Wolff DB, Adler RF, Gu G, Hong Y, Bowman KP, Stocker EF (2007) The TRMM multisatellite precipitation analysis (TMPA): quasi-global, multiyear, combined-sensor precipitation estimates at fine scales. *J Hydrometeorol* 8(1):38–55. <https://doi.org/10.1175/JHM560.1>
- Kalnay E, Lord SJ, McPherson RD (1998) Maturity of operational numerical weather prediction: medium range. *Bull Am Meteorol Soc* 79(12):2753–2770. [https://doi.org/10.1175/1520-0477\(1998\)079<2753:MOONWP>2.0.CO;2](https://doi.org/10.1175/1520-0477(1998)079<2753:MOONWP>2.0.CO;2)
- Karmakar N, Chakraborty A, Nanjundiah RS (2017) Space-time evolution of the low- and high-frequency intraseasonal modes of the Indian summer monsoon. *Mon Weather Rev* 145(2):413–435
- Krishnamurti T, Ardanuy P (1980) The 10 to 20-day westward propagating mode and “Breaks in the Monsoons”. *Tellus* 32(1):15–26. <https://doi.org/10.1111/j.2153-3490.1980.tb01717.x>
- Krishnamurti T, Kishtawal C, LaRow TE, Bachiochi DR, Zhang Z, Williford CE, Gadgil S, Surendran S (1999) Improved weather and seasonal climate forecasts from multimodel superensemble. *Science* 285(5433):1548–1550. <https://doi.org/10.1126/science.285.5433.1548>
- Lee Drbohlav HK, Krishnamurthy V (2010) Spatial structure, forecast errors, and predictability of the South Asian monsoon in CFS monthly retrospective forecasts. *J Clim* 23(18):4750–4769. <https://doi.org/10.1175/2010JCLI2356.1>
- Li Y, Han W, Wang W, Zhang L, Ravichandran M (2018) The Indian summer monsoon intraseasonal oscillations in CFSv2 forecasts: biases and importance of improving air-sea interaction processes. *J Clim* 31(14):5351–5370. <https://doi.org/10.1175/JCLI-D-17-0623.1>
- Mass CF, Ovens D, Westrick K, Colle BA (2002) Does increasing horizontal resolution produce more skillful forecasts? The results of two years of real-time numerical weather prediction over the Pacific Northwest. *Bull Am Meteorol Soc* 83(3):407–430. [https://doi.org/10.1175/1520-0477\(2002\)083<0407:DIHRPM>2.3.CO;2](https://doi.org/10.1175/1520-0477(2002)083<0407:DIHRPM>2.3.CO;2)
- Pavan V, Doblas-Reyes FJ (2000) Multi-model seasonal hindcasts over the euro-atlantic: skill scores and dynamic features. *Clim Dyn* 16(8):611–625. <https://doi.org/10.1007/s003820000063>
- Sahai AK, Abhilash S, Chattopadhyay R, Borah N, Joseph S, Sharmila S, Rajeevan M (2014) High-resolution operational monsoon forecasts: an objective assessment. *Clim Dyn* 44(11–12):3129–3140. <https://doi.org/10.1007/s00382-014-2210-9>
- Sikka D, Gadgil S (1980) On the maximum cloud zone and the ITCZ over Indian longitudes during the southwest monsoon. *Mon Weather Rev* 108(11):1840–1853. [https://doi.org/10.1175/1520-0493\(1980\)108<1840:OTMCZA>2.0.CO;2](https://doi.org/10.1175/1520-0493(1980)108<1840:OTMCZA>2.0.CO;2)
- Simmons AJ, Hollingsworth A (2002) Some aspects of the improvement in skill of numerical weather prediction. *Q J R Meteorol Soc* 128(580):647–677. <https://doi.org/10.1256/003590002321042135>
- Slingo J, Inness P, Neale R, Woolnough S, Yang G (2003) Scale interactions on diurnal to seasonal timescales and their relevance to model systematic errors. *Ann Geophys* 46:1
- Taraphdar S, Mukhopadhyay P, Leung LR, Landu K (2016) Prediction skill of tropical synoptic scale transients from ECMWF and NCEP ensemble prediction systems. *Math Clim Weather Forecast* 2:1. <https://doi.org/10.1515/mcwf-2016-0002>
- Tibaldi S, Palmer T, Branković Ć, Cubasch U (1990) Extended-range predictions with ECMWF models: influence of horizontal resolution on systematic error and forecast skill. *Q J R Meteorol Soc* 116(494):835–866. <https://doi.org/10.1002/qj.49711649404>
- Yang F (2017) Decomposition and attribution of forecast errors. 7 International Verification Methods Workshop Berlin, Germany. https://www.7thverificationworkshop.de/Presentation/META_4_Yang.pdf. Accessed 22 Apr 2018
- Yasunari T (1979) Cloudiness fluctuations associated with the Northern Hemisphere summer monsoon. *J Meteorol Soc Jpn Ser II* 57(3):227–242. https://doi.org/10.2151/jmsj1965.57.3_227

Publisher's Note Springer Nature remains neutral with regard to jurisdictional claims in published maps and institutional affiliations.